Optimization of grid configuration by investigating its effect on positive plate of lead-acid batteries via numerical modelingd

Ali Alagheband, Mohammadyousef Azimi, Hadi Hashemi, Mohammad Kalani, Davood Nakhaie

Corresponding author E-mail: Tech@sstco.biz

1-Introduction:

Regarding wide range and new applications of lead acid batteries, which all includes higher discharge rates during lifetime, huge efforts have been exerted to overcome different failure mechanisms [1-4]. As it is well-known these failures are mainly caused by positive plates (except from Cold-Cranking Ability) [5]. Therefore many attempts have been made to enhance the positive plate performance [6-9]. As the discharge rate increases, ohmic voltage losses in current collecting system become more important [10]. The configuration of grid wires and location of lug play an important role in minimizing the ohmic drop, which would give rise to uniform current distribution and provides more reaction sites on the electrode [11]. Therefore some researches have been conducted to examine the effect of grid configuration on its current and potential distribution through gird wires, both by mathematical modeling [10-14] and experimental work [15] , but still some crucial design features are not fully considered which this study proves them to be of utmost importance and by employing numerical modeling, grid design principles in literature [16] and some innovations has as its purpose to optimize them to achieve the best practical grid design.

2-Theory:

The molar flux of a charged species (j) in an electrolyte arises from three transport mechanisms, i.e. migration, diffusion and convection.

$$N_j = -z_j \mu_j F C_j \nabla \Phi - D_j \nabla C_j + C_j v \quad (1)$$

The total ionic current density (i) is given by assigning the charge to flux of each species and summing over all species:

$$i = F \sum_j z_j N_j \quad (2)$$

Considering no ionic concentration gradients in the electrolyte and the condition of electroneutrality in solution and in case when there is no homogenous reaction in the electrolyte involving the ionic species or its net effect is zero it could be said:

$$\sum i z_j \nabla C_j = 0 \ (3) \qquad \sum i z_j C_i = 0 \ (4) \qquad \check{N}i = 0 \ (5)$$

By defining Ϭ as the specific electrolyte conductivity

$$\sigma = -F^2 \sum_j z_j^2 \mu_j C_j \quad (6)$$

Eq. (3) becomes ohm's law for ion transport in electrolytes:

$$i = \sigma \nabla \Phi \quad (7)$$

This results in the Laplace equation,

$$\nabla^2 \Phi = 0 \quad (8)$$

The overall overpotential at the electrode is also given by:

$$\eta = E - E_e - \Phi \quad (9)$$

At insulator boundary:

$$\nabla \Phi = 0 \quad (10)$$

And potential in the solution adjacent to the electrode is equal to the potential on the electronic conductor: [11]

$$\Phi_0 + \Phi_m = \text{constant} \quad (11)$$

Fig 1 :

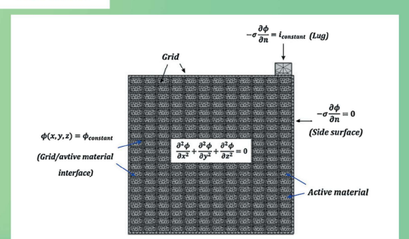

The equilibrium potential of the half-cell is:

$$E_{PbO_2/PbSO_4} = 1.683 - 0.118\ pH - 0.059 \lg a_{H_2O} + 0.029 \lg a_{SO_4^{2-}} \quad (2.E11)$$

In designing positive plates, there are some parameters which have to be taken into account.

A key parameter in designing battery plates is the ratio (α) between the grid weight (Wgrid) and the active mass weight (WPAM), i.e.,

$$\alpha = W_{grid}/(W_{PAM} + W_{grid}) \quad (12)$$

$$\gamma = W_{PAM}/S_{grid} \quad (13)$$

It is worth mentioning that the lower the Y value, the more grid surface and therefore the lower current density in high rate discharge [16].

The third parameter, β, is defined by the author as the ratio between the grid thickness and the plate thickness.

$$\beta = (\text{Plate Thickness-Grid Thickness})/\text{Grid Thickness} \quad (14)$$

3-Model

Founded on the theory explained in Section 2 and with employing Comsol software, a 3D numerical model has been developed to investigate the potential and current density distribution of twelve different grid configurations shown in Fig 3. The specifications of six described models are depicted in Table 2. The grid boundaries were set as insulator where the current applied to the surface was zero. 100 A was introduced to the lug of each grid in the model. The model was solved in stationary state. [12]

Fig 2 :

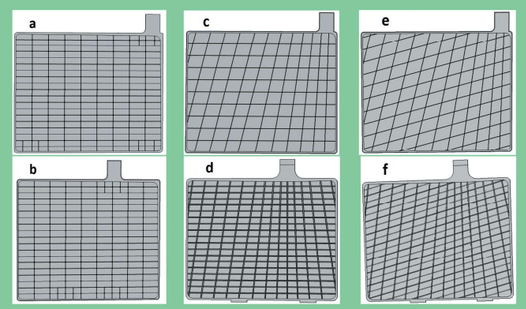

Table 1 :

Models	Grid Weight (g)	PAM Weight (g)	α	β (g/cm²)	Y
Conventional Side-lug	55.05	97.5	0.361	0.266	0.761
Conventional Middle-lug	55.04	97.5	0.361	0.266	0.760
Diagonal Side-lug	55.04	97.5	0.361	0.265	0.755
Diagonal Middle-lug	55.04	97.5	0.361	0.265	0.754
Double-diagonal Side-lug	55.05	97.5	0.361	0.261	0.751
Double-diagonal Middle-lug	55.03	97.5	0.361	0.26	0.749

4. Results and discussion

Fig. 3 shows the potential distribution in the six described electrodes. Maximum and minimum values as well as potential differences for all models are listed in table 3. Although the maximum value for all cases is almost the same, the minimum value is completely different. Potential values in diagonal and double-diagonal configurations are not as low as conventional design near the lug regardless to its lug position.

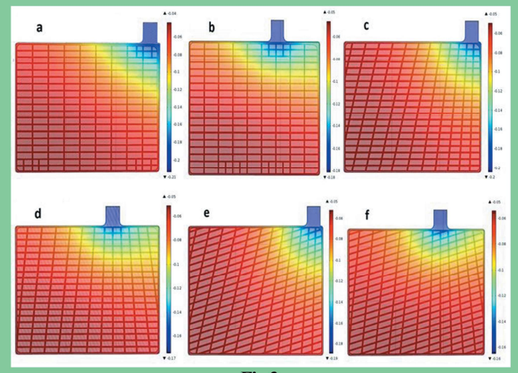

Fig 3

Table 2

Grid name	E_{min} (V)	E_{max} (V)	ΔE (mV)
Conventional Side-Lug	-0.21	-0.04	170
Conventional Middle-Lug	-0.18	-0.05	130
Diagonal Side-Lug	-0.2	-0.05	150
Diagonal Middle-Lug	-0.17	-0.05	120
double-diagonal Side-Lug	-0.19	-0.05	140
double-diagonal Middle-Lug	-0.16	-0.05	110

Potential distributions through the active material and adjacent electrolyte to the grid are illustrated in Fig 4. Since outer boundaries of electrolyte domain are set as insulators, their potential values assume to be zero. Maximum and minimum potential values and their differences are presented in table 4. It can conclusively be gathered that it projects a same trend with potential distribution in grid surface.

Table 3

Grid name	E_{min} (V)	E_{max} (V)	ΔE (mV)
Conventional Side-Lug	-0.19	-0.048	142
Conventional Middle-Lug	-0.161	-0.052	109
Diagonal Side-Lug	-0.181	-0.053	128
Diagonal Middle-Lug	-0.152	-0.054	98
double-diagonal Side-Lug	-0.167	-0.056	111
double-diagonal Middle-Lug	-0.143	-0.057	86

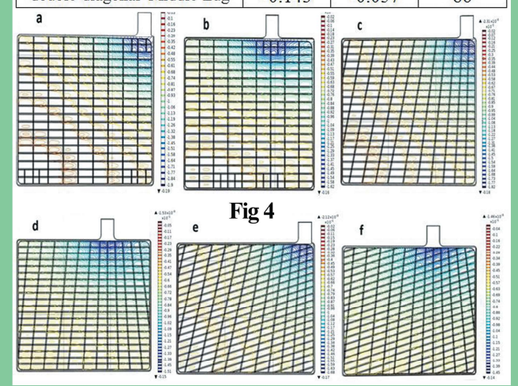

Fig 4

The effect of grid configuration and lug position on the distribution of current density in the electrolyte adjacent to surface of each plate has been shown in Fig. 5. Max and min values of current density in the electrolyte are tabulated in Table 5. Since the whole current produced in a battery plate passes through the lug, this section carries highest current density value.

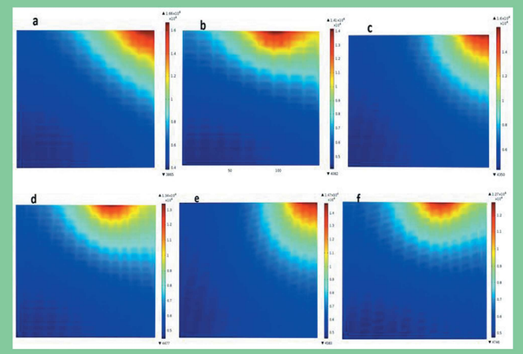

Fig 5

Table 4

Grid name	i_{min} (A/m²)	i_{max} (A/m²)	Δi (A/m²)
Conventional Side-Lug	3865	16600	12735
Conventional Middle-Lug	4082	14100	10018
Diagonal Side-Lug	4350	16000	11650
Diagonal Middle-Lug	4477	13400	8923
double-diagonal Side-Lug	4583	14700	10117
double-diagonal Middle-Lug	4746	12700	7954

Further Improvement

Some design parameters have been chosen including the level of tapering vertical wires toward lug, the angle of skewing the horizontal wires and the position of lug. The weight in these grids is 49g which is 6g less than all previous ones. Table 5 provides design specifications for new models. Final results are reported here in Table 6.

Table 5

	Modifications	Weight	α	B	Y
A	Horizontal wires angle :14	49.07	0.335	0.24	0.718
B	Horizontal wires angle :15	49.02	0.335	0.24	0.702
C	Horizontal wires angle :16	49.02	0.335	0.239	0.718
D	Lug position CC=50	49.02	0.335	0.24	0.702
E	Lug position CC=55	49.02	0.335	0.24	0.718
F	Lug position CC=60	49.02	0.335	0.24	0.719
G	Tapering Level : A	49	0.334	0.239	0.717
H	Tapering Level : B	49.02	0.335	0.24	0.702
I	Tapering Level : C	49.12	0.335	0.238	0.722

Table 6

	Difference in grid potential (mV)	Difference in AM and adjacent electrolyte potential (mV)	Difference in current density (A/m²)	Maximum current density (A/m²)
A	110	88	12800	7967
B	110	86	12700	7954
C	120	89	12800	7981
D	110	86	12700	7954
E	110	89	12800	7969
F	120	91	12800	7991
G	120	89	12800	7972
H	110	86	12700	7954
I	120	90	12900	8001

References:

[1] S. Fouache, A. Chabrol, G. Fossati, M. Bassini, M.L. Sainz, L. Atkins,J. Power Sources 78 (1999) 12.
[2] M. Metikoš-Hukovi´c, R. Babi´c, S. Brini´c, J. Power Sources 64 (1997) 13.
[3] L. Albert, A. Gegaudin, E. Julliam, J. Power Sources 78 (1999) 12.
[4] P.T. Moseley, J. Power Sources 64 (1997) 47.
[5] Yongfang Guo, Yi Li, Guoshong Zhang, Huixiang Zhang, J. Guo,he J. Power Sources 124 (2003) 271–277.
[6] R.D. Prengaman, Journal of Power Sources 95 (2001) 224–233.
[7] S. Fouache, A. Chabrol, G. Fossati, M. Bassini, M.L. Sainz, L. Atkins, Journal ofPower Sources 78 (1999) 12–22.
[8] J.E. Manders, N. Bui, D.W.H. Lambert, J. Navarette, R.F. Nelson, E.M. Valeriote,Journal of Power Sources 73 (1998) 152–161.
[9] R. Pourraj, S.D. McAllister, I.F. Cheng, D.B. Edwards, Journal of Power Sources189 (2009) 1199–1203.
[10] Eberhard Meissner, S.D. McAllister, I.F. Cheng, D.B. Edwards, Journal of Power Sources 42(1993) 103-118.
[11] D. Nakhaie, P.H. Benhangi, A. Alfantazi, A. Davoodi, Electrochimica Acta 115 (2014) 189-196
[12] K. Yamada, K.-i. Maeda, K. Sasaki, T. Hirasawa, Journal of Power Sources 144(2005) 352–357
[13] R.J. Ball, R.Evans, R. Stevens, Journal of Power Sources 103(2002)213-222
[14] G.J. May, N. Maleschitz, H. Diermaier, T. Haeupl, Journal of Power Sources 195(2010) 4520–4524.
[15] M. Calábek, K. Micka, P. Ba'ca, P. K'rivák, Journal of Power Sources 85 (2000)145–148.
[16] D. Pavlov, J. Power Sources 53 (1995) 9.